Mon. Not. R. Astron. Soc. **000**, 1–9 (2007) Printed 1 February 2008 (MN LATEX style file v2.2)

A double main sequence turn-off in the rich star cluster NGC 1846 in the Large Magellanic Cloud

A. D. Mackey[1] and P. Broby Nielsen[1]
[1] *Institute for Astronomy, University of Edinburgh, Royal Observatory, Blackford Hill, Edinburgh, EH9 3HJ, UK*

arXiv:0704.3360v1 [astro-ph] 25 Apr 2007

Draft version 1 February 2008

ABSTRACT

We report on HST/ACS photometry of the rich intermediate-age star cluster NGC 1846 in the Large Magellanic Cloud, which clearly reveals the presence of a double main sequence turn-off in this object. Despite this, the main sequence, sub-giant branch, and red giant branch are all narrow and well-defined, and the red clump is compact. We examine the spatial distribution of turn-off stars and demonstrate that all belong to NGC 1846 rather than to any field star population. In addition, the spatial distributions of the two sets of turn-off stars may exhibit different central concentrations and some asymmetries. By fitting isochrones, we show that the properties of the colour-magnitude diagram can be explained if there are two stellar populations of equivalent metal abundance in NGC 1846, differing in age by ≈ 300 Myr. The absolute ages of the two populations are ~ 1.9 and ~ 2.2 Gyr, although there may be a systematic error of up to ± 0.4 Gyr in these values. The metal abundance inferred from isochrone fitting is [M/H] ≈ -0.40, consistent with spectroscopic measurements of [Fe/H]. We propose that the observed properties of NGC 1846 can be explained if this object originated via the tidal capture of two star clusters formed separately in a star cluster group in a single giant molecular cloud. This scenario accounts naturally for the age difference and uniform metallicity of the two member populations, as well as the differences in their spatial distributions.

Key words: globular clusters: individual: NGC 1846 – Magellanic Clouds – galaxies: star clusters.

1 INTRODUCTION

The Large Magellanic Cloud (LMC) possesses an extensive system of massive star clusters, covering the full range of ages $10^6 - 10^{10}$ yr. This age spread, which is not present in the Galactic globular cluster population, combined with the close proximity of the LMC system, means that these objects have proved vital to our understanding of star cluster formation and evolution. Furthermore, the age and metallicity distributions of the LMC clusters, together with their kinematics, offer important insights into the formation and subsequent development of the LMC itself.

As part of a study of the structural evolution of massive stellar clusters, we have conducted a snapshot imaging survey of some ~ 50 such objects in the LMC and SMC using the Advanced Camera for Surveys (ACS) on-board the Hubble Space Telescope (HST). Many of the target clusters have not previously been investigated in any detail, and we are therefore working on deriving accurate photometric ages and metallicities for the sample (Mackey & Gilmore 2004; Mackey, Payne & Gilmore 2006). While reducing our observations of the poorly-studied rich intermediate-age LMC cluster NGC 1846, we recently noticed that the colour-magnitude diagram (CMD) for this object exhibited a very peculiar main sequence turn-off region; further scrutiny revealed clearly the presence of two distinct turn-offs. With a few notable exceptions (for example, the massive Galactic globular cluster ω Centauri), the vast majority of star clusters which have been resolved by observations into individual stars are comprised of single stellar populations – that is, groups of stars formed at the same time and with the same chemical composition. NGC 1846 is therefore an important object, as it can potentially offer us new insights into the processes of star and star cluster formation.

In this paper we present our photometry of NGC 1846 together with a detailed investigation of its extremely unusual CMD (Sections 2 and 3.1). We examine the spatial distribution of stars in the main sequence turn-off region, and demonstrate that both turn-offs are clearly associated with the cluster rather than being an artifact introduced by field star contamination (Section 3.2). In addition, we show that neither differential reddening, nor a significant line-of-sight depth to NGC 1846 can explain the double turn-off. From isochrone fitting, we determine the ages and metallicities of the two populations present in NGC 1846 (Section 3.3), and use these results to constrain the possible means by which this object can have been formed (Section 4).

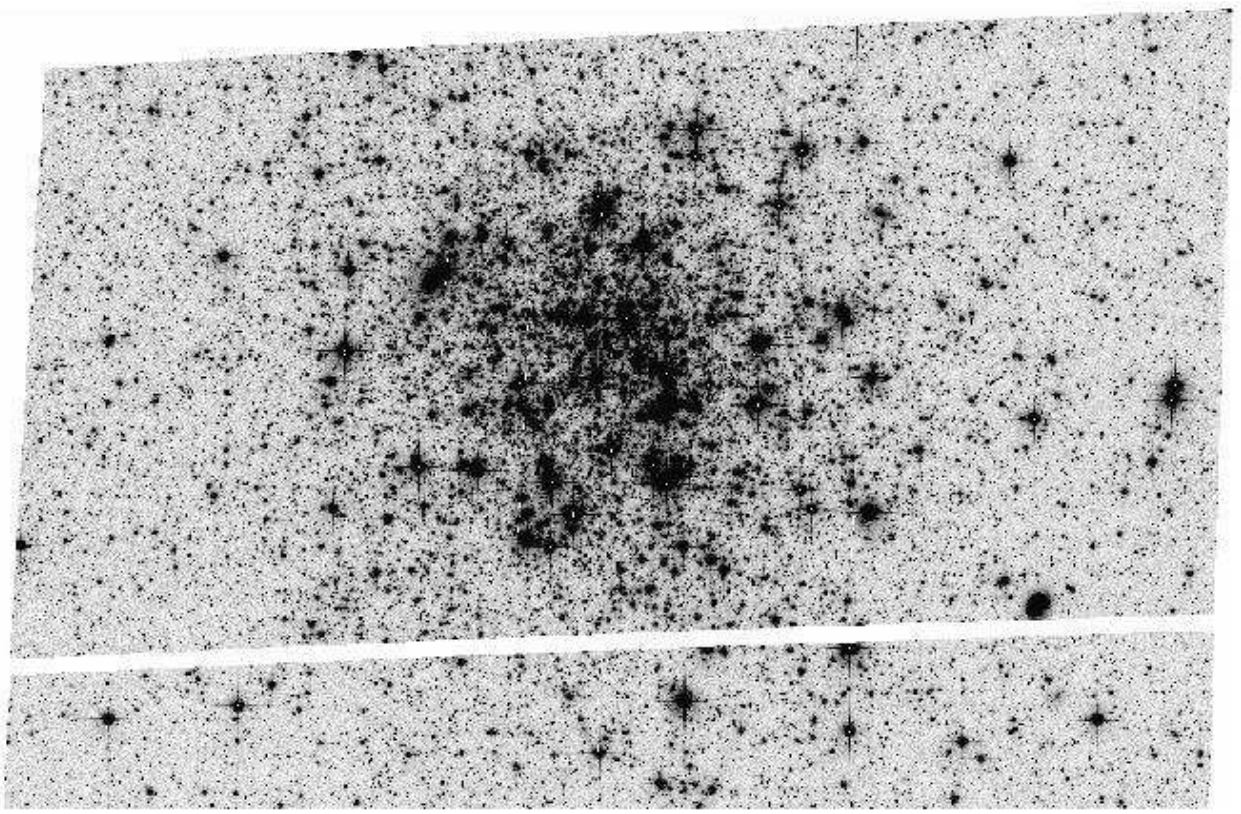

Figure 1. Drizzled ACS/WFC F814W image of the core of NGC 1846 (exposure 200s). The full image has been cropped to include only WFC chip 1 and part of WFC chip 2 – these cover the central cluster region. Note that the brightest stars in the cluster are saturated.

2 OBSERVATIONS AND DATA REDUCTION

Our observations were made during HST Cycle 12 on 2003 October 08 using the ACS Wide Field Channel (WFC). As a snapshot target, one frame was taken in each of two filters – F555W (dataset j8ne55z9q) and F814W (dataset j8ne55zeq). Exposure durations were 300s and 200s, respectively. The ACS WFC consists of two 2048×4096 pixel CCDs separated by a gap ≈ 50 pixels wide. The plate scale is 0.05 arcsec per pixel, resulting in a total areal coverage of approximately 202×202 arcsec. The core of NGC 1846 was positioned at the centre of chip 1 so that the inter-chip gap did not impact on the innermost region of the cluster. In order to help with the identification and removal of hot-pixels and cosmic rays, the F814W image was offset from the F555W image by ≈ 2 pixels in both the x- and y-directions.

The data products produced by the STScI reduction pipeline, which we retrieved via the public archive, have had bias and dark-current frames subtracted and are divided by a flat-field image. In addition, known hot-pixels and other defects are masked, and the photometric keywords in the image headers are calculated. We also obtained distortion-corrected (drizzled) images from the archive, produced using the PYRAF task MULTIDRIZZLE. Part of the drizzled F814W image is displayed in Fig. 1.

We used the DOLPHOT photometry software (Dolphin 2000), specifically the ACS module, to photometer our flatfielded F555W and F814W images. DOLPHOT performs point-spread function fitting using PSFs especially tailored to the ACS camera. Before performing the photometry, we first prepared the images using the DOLPHOT packages ACSMASK and SPLITGROUPS. Respectively, these two packages apply the image defect mask and then split the multi-image STScI FITS files into a single FITS file per chip. We then used the main DOLPHOT routine to simultaneously make photometric measurements on the pre-processed images, relative to the coordinate system of the drizzled F814W image. We chose to fit the sky locally around each detected source (important due to the crowded nature of the target), and keep only objects with a signal greater than 10 times the standard deviation of the background. The output photometry from DOLPHOT is on the calibrated VEGAMAG scale of Sirianni et al. (2005), and corrected for charge-transfer efficiency (CTE) degradation.

To obtain a clean list of stellar detections with high quality photometry, we applied a filter employing the sharpness and "crowding" parameters calculated by DOLPHOT. The sharpness is a measure of the broadness of a detected object relative to the PSF – for a perfectly-fit star this parameter is zero, while it is negative for an object which is too sharp (perhaps a cosmic-ray) and positive for an object which is too broad (say, a background galaxy). The crowding parameter measures how much brighter a detected object would have been measured had nearby objects not been fit simultaneously. We selected only objects with $-0.15 \leqslant$ sharpness $\leqslant 0.15$ in both frames, and crowding $\leqslant 0.5$ mag in both frames. We also only kept objects classified

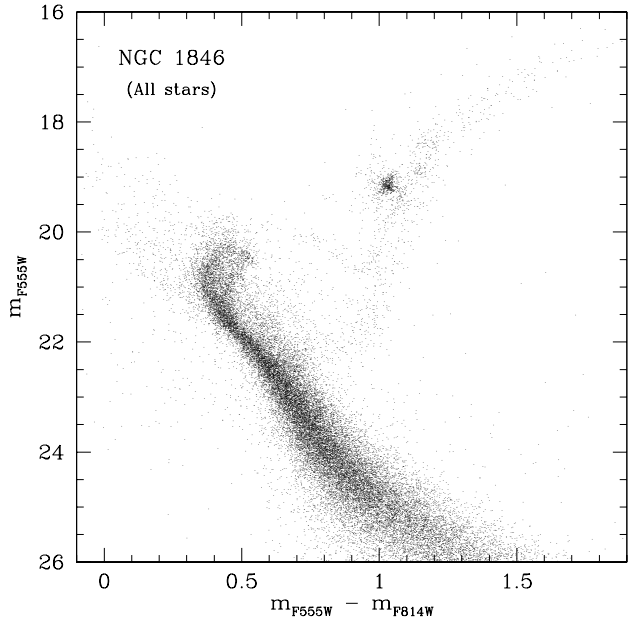

Figure 2. Colour-magnitude diagram for NGC 1846. All detected sources which passed successfully through our quality filter are plotted (34534 objects). The main cluster sequences are clearly visible; however there is some field star contamination present in key regions, particularly along the RGB and main sequence. Even so, the double main sequence turn-off is strikingly evident.

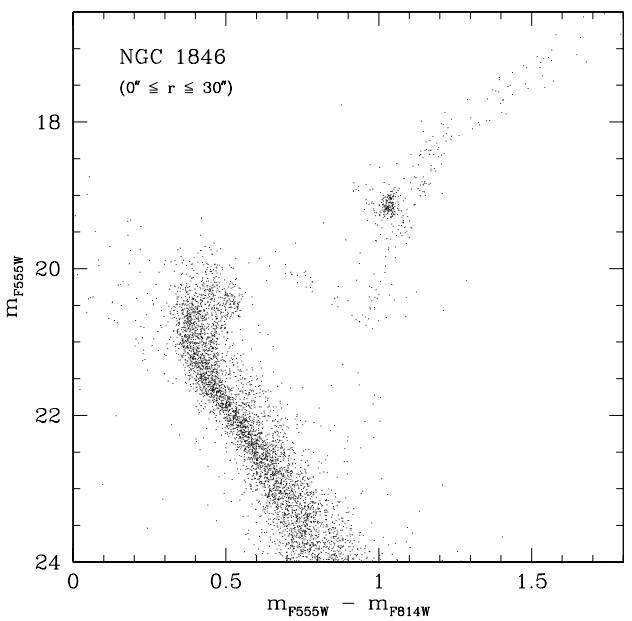

Figure 3. Colour-magnitude diagram for NGC 1846, now plotted using only quality-filtered stars at projected radial distances less than 30″ from the centre (6599 objects). The majority of field star contamination has been removed leaving the cluster sequences clearly visible, particularly the double main sequence turn-off. Note that the view in this plot is focussed on the turn-off region, SGB and RGB, so the scale is different from that of Fig. 2.

by DOLPHOT as good stars (object type 1), as opposed to elongated or extended objects (object types > 1).

3 RESULTS

3.1 Colour-magnitude diagram

The colour-magnitude diagram (CMD) for NGC 1846 is presented in Fig. 2. All detected stars which passed successfully through the quality filter are plotted. There is some evident field-star contamination present in this CMD, so in Fig. 3 we plot only stars within 30″ of the cluster centre, which lies near pixel coordinates $(x_c, y_c) = (2120, 3150)$ (see Section 3.2 below). Since this selected region is very much smaller in area than the full ACS coverage, field-star contamination in the CMD is greatly reduced compared to Fig. 2 and allows one to clearly identify the primary cluster sequences. In principle we could apply a more sophisticated statistical subtraction of field stars; however this is unnecessary to achieve the goals of the present work. Selecting the innermost cluster regions, as in Fig. 3, clearly offers a sufficiently uncontaminated CMD.

The most striking and unusual feature of the CMD for NGC 1846 is the presence of an apparently double main sequence turn-off. This is clearly visible in both Figs. 2 and 3, suggesting it is not an artifact of field star contamination (we address this issue more completely in Section 3.2 below). Apart from this, the CMD is as expected for an intermediate-age Magellanic Cloud cluster. There is a relatively narrow main sequence, a down-sloping sub-giant branch (SGB), and a narrow red giant branch (RGB), as well as a compact red clump (RC) near $m_{\rm F555W} \approx 19.1$ and $m_{\rm F555W} - m_{\rm F814W} \approx 1.0$. On the RGB just brighter than the RC level a clear knot of stars is visible, especially in Figure 2. This is possibly the RGB Bump – the point at which the hydrogen-burning shell in a red giant star reaches the discontinuity left in the hydrogen abundance profile due to inner penetration of convection. A similar feature has recently been observed in the rich intermediate-age LMC cluster NGC 1978 by Mucciarelli et al. (2007) – an object which presents a very similar CMD to that for NGC 1846 (although without the double main sequence turn-off).

It is worth noting that a third turn-off is clearly visible in Fig. 2, near $m_{\rm F555W} \sim 22.5$. This is clearly part of the contaminating field star population (since it disappears in Fig. 3), and is representative of a much older population than that present in NGC 1846. Mucciarelli et al. (2007) observe a similar population in the field surrounding NGC 1978, and interpret it as the signature of a major star formation episode which occurred $\sim 5 - 6$ Gyr ago when the LMC and SMC were gravitationally bound.

Above $m_{\rm F555W} \approx 18.0$, the width of the cluster RGB appears to increase significantly. Examining the data quality flags produced by DOLPHOT we found that all stars above this level were flagged as being saturated in their central pixels (see e.g., the brightest stars in Fig. 1). The accuracy of all photometry on the RGB above $m_{\rm F555W} = 18.0$ is therefore dubious, and the apparent increased spread is most likely artificial.

Based on an unpublished CMD, Grocholski et al. (2006) suggested that NGC 1846 suffers from differential reddening; however, from the narrow (lower) RGB and the compact RC visible in Fig. 3 we see no evidence for significant differential

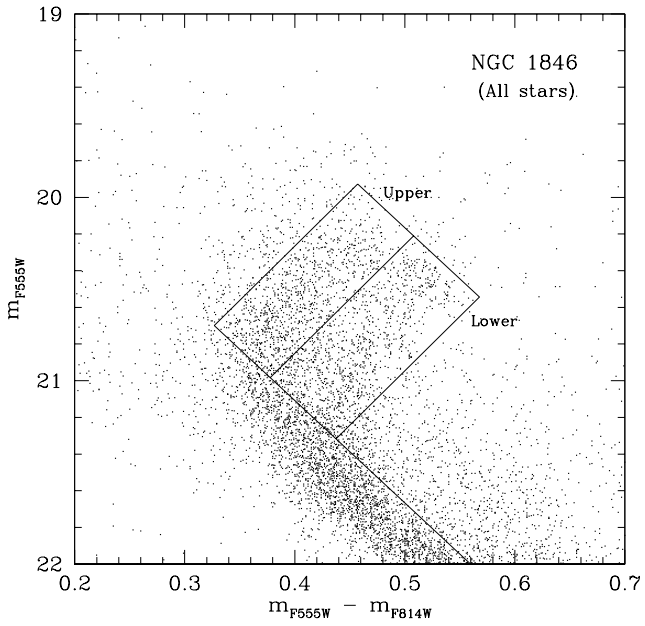

Figure 4. Colour-magnitude diagram of the main sequence turn-off region of NGC 1846, with all stars plotted as in Fig. 2. The two marked boxes were determined empirically using the CMD in Fig. 3 and are designed to isolate the "upper" and "lower" turn-off stars. The main sequence itself has been excluded to try and maintain as clean a separation as possible.

reddening, at least in the central regions of the cluster. Certainly the apparent double main sequence turn-off cannot be produced by such an effect without introducing a large spread into the other features on the cluster CMD. Similarly, the observed lack of such a spread in these features militates against a large line-of-sight depth in the system being responsible for the properties of the turn-off region.

3.2 Spatial distribution of turn-off stars

The most intriguing aspect of the CMD for NGC 1846 is the double main sequence turn-off. Such a clearly defined example has not previously been observed in a Magellanic Cloud cluster – indeed, it is rare to find such a feature in *any* type of star cluster. The turn-off region is suggestive of two separate cluster populations. If this is so then it is important to ascertain whether there are any differences in their spatial distributions, as is observed, for example, for the multiple populations found in the peculiar Galactic globular cluster ω Centauri (see e.g., Villanova et al. 2007, and references therein).

We first need to demonstrate that all stars in the main sequence turn-off region belong to the cluster. To this end, we used Fig. 3 to isolate the areas on the CMD covered by the two visible turn-offs. We then searched through the full list of stars plotted in Fig. 2 and chose only those lying in these two regions. The results of this process are displayed in Fig. 4. The two boxes define the sets of "upper" and "lower" turn-off stars. By examining the spatial distributions of these two ensembles, we can check that they both

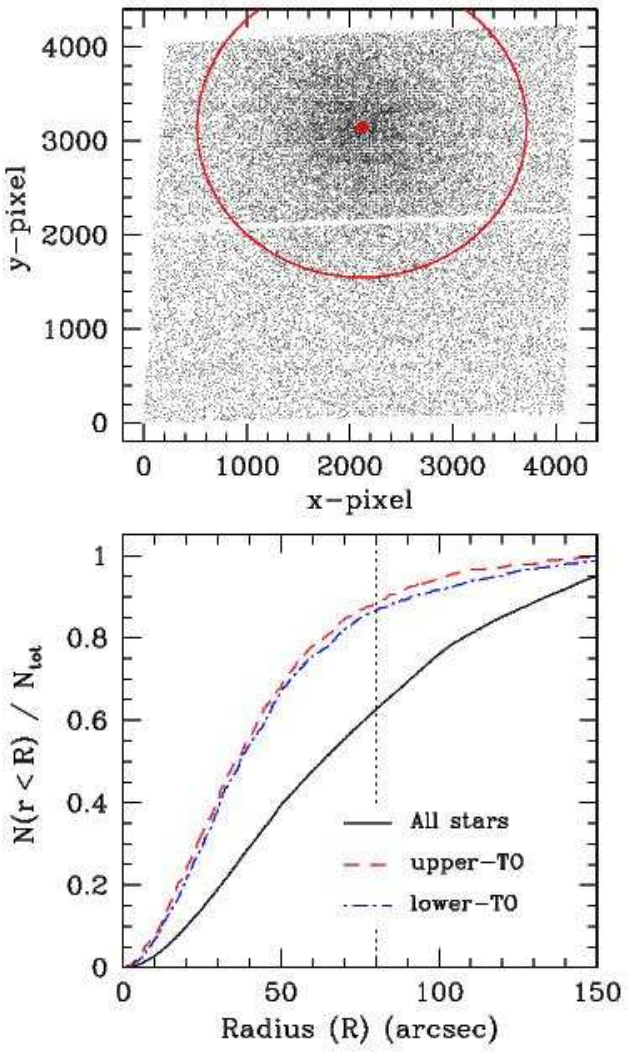

Figure 5. Upper panel: Pixel coordinates of all 34534 detected stars with high quality photometry, along with our measured centre at $(x_c, y_c) = (2120, 3150)$ (solid point). The solid circle marks a radius of $80''$ (1600 pixels) about this centre. **Lower panel:** Distributions of projected radial distance from the cluster centre for all stars (solid line), upper turn-off stars (dashed line), and lower turn-off stars (dot-dashed line). The vertical dotted line marks a radius of $80''$, as plotted in the upper panel. Approximately 90 per cent of the turn-off stars lie within this radius.

do belong to the cluster, and search for differences between them.

In Fig. 5 we plot the distribution of projected radial distance from the cluster centre for all stars and compare this with the distributions of projected radial distance from the cluster centre for the upper and lower turn-off stars. We determined the cluster centre using a surface-brightness testing algorithm very similar to that described by Mackey & Gilmore (2003), with the result that the cluster centre lies within ≈ 20 pixels ($1''$) of the pixel coordinates $(x_c, y_c) = (2120, 3150)$. The pixel coordinates of all stars are plotted in the upper panel of Fig. 5 along with a point marking the measured cluster centre.

The radial distribution of all stars (including both cluster and field stars), plotted as a solid line in the lower panel

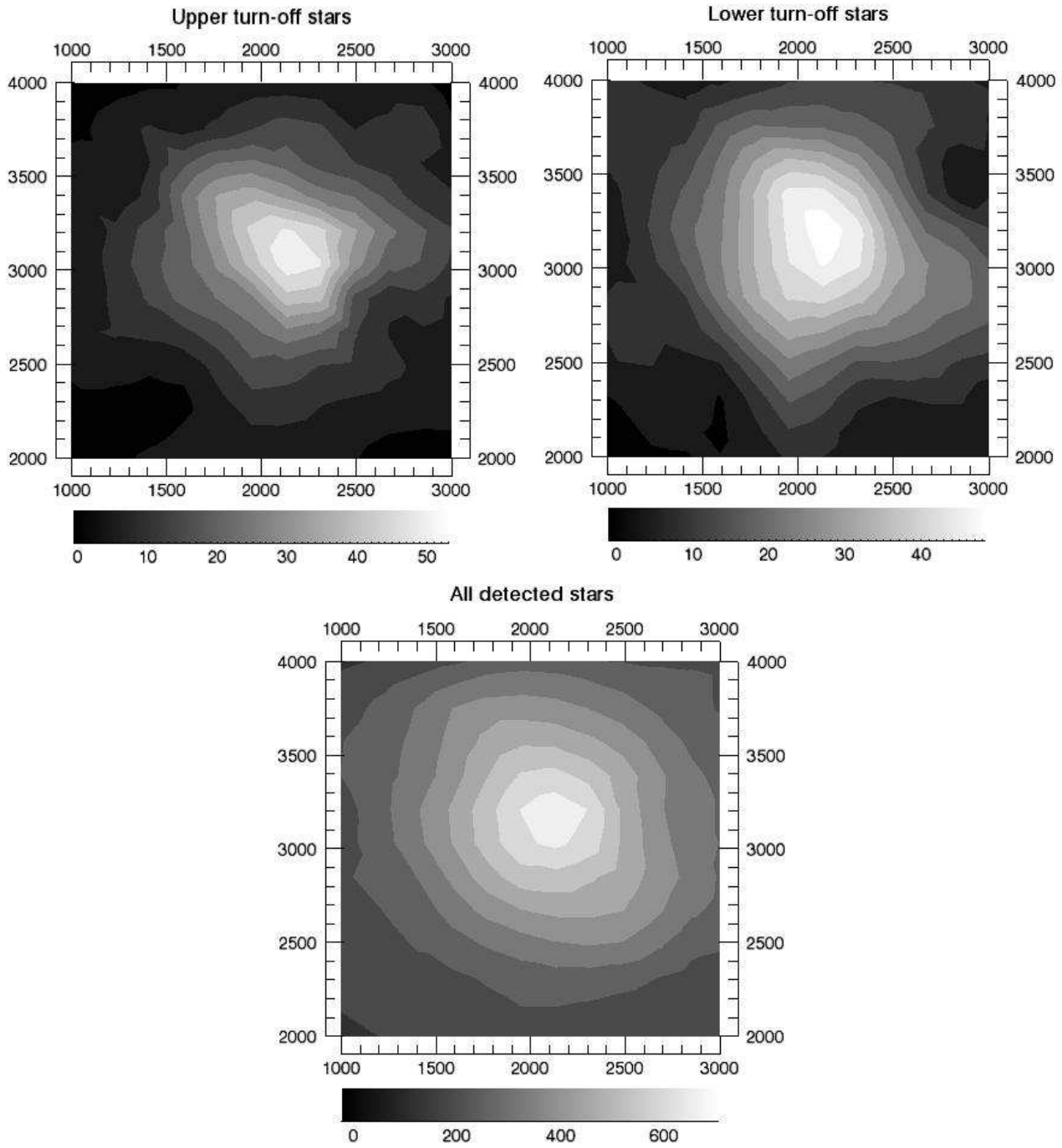

Figure 6. Contour plots of the spatial distribution of upper turn-off stars (top left panel), lower turn-off stars (top right panel), and all detected stars (lower panel). Axis units are pixel coordinates – the plots are zoomed on the cluster centre, so do not cover the entire ACS field of view. They were produced by calculating a 2D histogram of stellar positions using a box size of 300 × 300 pixels, and then smoothing and contouring the result. The marked contours in the upper two panels delineate approximately equivalent density levels.

of Fig. 5, is much less centrally concentrated than those of the upper and lower turn-off stars (dashed line, and dot-dashed line, respectively). Approximately 90 per cent of the turn-off stars lie within a radius of $\sim 80''$ (1600 pixels) of the cluster centre, as marked in the upper panel of the Figure. This observation strongly implies that these objects are associated with the cluster itself rather than representing any type of field star contamination. There is also apparently a small difference between the radial distributions of the two sets of turn-off stars, suggesting that the lower turn-off stars may be a little less centrally concentrated than the upper turn-off stars.

In Fig. 6, we show contour plots of the spatial distributions of all stars (lower panel) and of both sets of turn-off

stars (upper two panels). This allows us to further compare the spatial distributions of the turn-off stars to each other and to the rest of the cluster stars. We produced each plot by first making a 2D histogram of the pixel coordinates of the stars in the relevant group, using a bin size of 300×300 pixels. Selection of this size represents a trade-off between high spatial resolution and having a significant number of stars per bin for the turn-off plots; we retained the same box size for the plot including all stars to allow direct comparison. After calculating the histogram we smoothed the result using the MIN_CURVE_SURF function in IDL, and then obtained a contour map using the CONTOUR procedure in IDL. The results still inevitably contain a small amount of residual boxiness from the 2D histogram; however this does not affect the overall shapes and spacing of the displayed contours.

The lower panel of Fig. 6 shows that the cluster considered as a whole appears to be relatively smoothly and symmetrically distributed. The centre matches well our measured value of $(x_c, y_c) = (2120, 3150)$, and there is no strong evidence for significant ellipticity or clumpiness. From the upper two panels, it is clear that the two sets of turn-off stars are very definitely associated with the cluster, as we surmised from Fig. 5. In addition, within the accuracy of centroiding from the maps (roughly ± 50 pixels, or $\pm 2.5''$) their centres are coincident with each other and the cluster as a whole. It is possible that the set of upper turn-off stars is more centrally concentrated than both the set of lower turn-off stars and the cluster as a whole (this would be consistent with Fig. 5), and furthermore, that the distribution of upper turn-off stars may also exhibit some significant asymmetry. However, both improved photometry of the turn-off region and a more sophisticated statistical analysis are required to draw a firm conclusion on these issues.

Together Figs. 5 and 6 offer strong evidence that both sets of turn-off stars are definitely associated with NGC 1846 rather than any field star population. Furthermore, there are tantalizing indications that the spatial distributions of the two sets of turn-off stars may be somewhat different to each other, although improved measurements are required to confirm this.

3.3 Isochrone fitting

From the above analysis, we conclude that the observed double main sequence turn-off in NGC 1846 results from the presence of two separate stellar populations in this cluster. However, even though the two main sequence turn-offs are quite distinct, the RGB (below the saturation level at $m_{\rm F555W} = 18.0$) is narrow, and the RC is of a compact nature. This implies that the two populations cannot be of strongly differing metallicities, since both the RGB and the RC of a more metal rich population would lie considerably further to the red than those for a more metal poor population, and the RC would also be somewhat less luminous for the more metal rich population than for the metal poor population.

To quantify the main characteristics (age, metallicity) of the two populations in NGC 1846, we fit isochrones to the cluster CMD. We used two sets of stellar models which have isochrones calculated in the F555W and F814W ACS/WFC filter systems – those of the Padova group (Girardi et al. 2000), and those from the BaSTI evolutionary code (Pietrinferni et al. 2004; Bedin et al. 2005). We selected the "basic set" of Padova tracks with solar-scaled distribution of metals (in particular, that is, not enhanced in α-elements), which include some degree of convective overshooting (for details see Girardi et al. 2000), and the "non-canonical" solar-scaled BaSTI tracks, which also employ convective overshooting (see Pietrinferni et al. 2004).

Apart from the double turn-off, NGC 1846 presents a rather similar CMD to that of NGC 1978, which was recently measured to be 1.9 ± 0.1 Gyr old (Mucciarelli et al. 2007). There are two available spectroscopic measurements of the metallicity of NGC 1846 – that of Olszewski et al. (1991) who found $[{\rm Fe/H}] = -0.70 \pm 0.20$ from one RGB star, and that of Grocholski et al. (2006) who obtained $[{\rm Fe/H}] = -0.49 \pm 0.03$ from 17 RGB stars. For the Padova models we used the interactive web form available on the group's web site to construct a fine grid of isochrones about these values, sampling an age range $1.0 \leqslant \tau \leqslant 3.0$ Gyr at intervals of 0.1 Gyr, and a metal abundance range $0.00250 \leqslant Z \leqslant 0.00950$ at intervals of 0.00025. The total metallicity $[{\rm M/H}] = \log(Z/Z_\odot)$ where $Z_\odot \approx 0.019$, so this abundance range corresponds to $-0.88 \leqslant [{\rm M/H}] \leqslant -0.30$. Assuming the α-element enhancement in NGC 1846 is small, which would be consistent with other intermediate-age LMC clusters (see e.g. Mucciarelli et al. 2007, for NGC 1978), then $[{\rm M/H}] \sim [{\rm Fe/H}]$. For the BaSTI tracks, we used the web form available on that group's web site to construct a grid of isochrones sampling the same age range as the Padova grid, at the same intervals, but for only two metal abundances – $Z = 0.004$ and $Z = 0.008$ (the BaSTI web form does not allow interpolation in metal abundance).

We first attempted to find the best fitting isochrone for the upper main sequence turn-off. We did this by locating by eye three fiducial points on the CMD of the cluster's central region: the magnitude and colour of the turn-off, the magnitude of the RC, and the colour of the RGB at a level 1.0 mag brighter than the level of the turn-off. This latter point was selected simply as a point lying on the lower RGB at a level intermediate between that of the red end of the SGB and that of the RC. We then calculated the intervals $\Delta_{\rm V}$ and $\Delta_{\rm C}$, which are, respectively, the difference in magnitude between the level of the turn-off and the level of the RC, and the difference in colour between the turn-off and the RGB fiducial point. These intervals are useful because $\Delta_{\rm V}$ is strongly sensitive to cluster age (and weakly to cluster metallicity), while $\Delta_{\rm C}$ is sensitive to both cluster age and metallicity. We obtained $\Delta_{\rm V} = 1.65 \pm 0.1$ mag and $\Delta_{\rm C} = 0.68 \pm 0.01$ mag.

Next, we calculated the same intervals for all isochrones on each of our two grids, and selected only those with values lying within certain tolerances of the cluster measurements (± 0.2 mag for $\Delta_{\rm V}$ and ± 0.02 mag for $\Delta_{\rm C}$). This resulted in lists of fewer than ten isochrones per grid, which we then fit to the CMD by eye. To do this, we calculated the offsets in magnitude and colour required to align the turn-off of the isochrone with that of the CMD, and then those required to align the RC of the isochrone with that of the CMD. This resulted in two offsets in magnitude, and two offsets in colour, which we averaged and then applied to overplot the isochrone on the CMD. Given the narrowness of most of the sequences on the CMD, it was then straightforward to

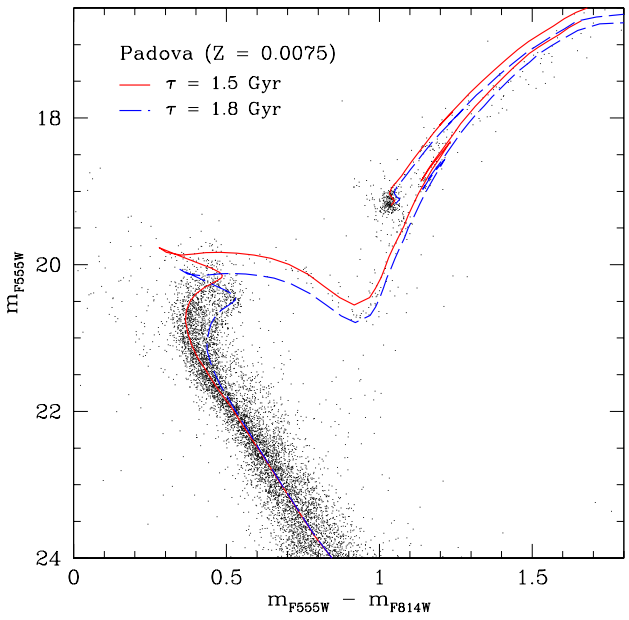

Figure 7. Best-fitting Padova isochrones overplotted on the cluster CMD. The upper and lower turn-off isochrones have the same metal abundance $Z = 0.0075$, and ages $\tau_u = 1.5$ Gyr and $\tau_l = 1.8$ Gyr, respectively. Both have been shifted by $E(V-I) = 0.045$ and $\mu = 18.37$ to achieve the best-fitting alignment.

identify the best fitting isochrone for each grid. The resulting offsets δ_V and δ_C provide estimates for the distance modulus to the cluster (μ) and the foreground extinction, in that $\delta_C = E(m_{F555W} - m_{F814W}) \approx E(V-I)$ (since the extinction values are small, see Sirianni et al. 2005) and $\delta_V = \mu + 2.37E(V-I)$.

We then moved to the lower turn-off and repeated the above process. In Section 3.2, we demonstrated that both populations in NGC 1846 share an approximately common spatial centre. Furthermore, the narrowness of the CMD sequences implies that there is little or no differential reddening towards the cluster centre, nor a significant line-of-sight depth to the system. In aligning the best-fitting isochrones to the lower turn-off, we therefore applied the same distance modulus and extinction values calculated for the upper turn-off.

The best-fitting Padova isochrones may be seen in Fig. 7. We found that the highest quality solution was for isochrones of the same metal abundance ($Z = 0.0075$, or [M/H] $= -0.40$) but differing ages: $\tau_u = 1.5$ Gyr for the upper turn-off and $\tau_l = 1.8$ Gyr for the lower turn-off. The isochrone filtering process outlined above provided an indication of the random uncertainties associated with these results – isochrones with ± 0.00025 in Z and ± 0.1 Gyr in age gave reasonable fits, but clearly not as good as for the selected values. The fact that the two isochrones have the same metallicity is primarily driven by the narrowness of the observed RGB and the compact nature of the RC. Matching these features is successfully achieved if there is solely an age difference between the two populations. The observed width of the SGB is successfully matched at the red end, but is apparently a little too wide at the blue end. The reason for this is not clear – it may represent a shortcoming of the stellar models (although we note that the Basti isochrones also predict too wide an SGB at the blue end), or may represent another very unusual feature of the CMD for NGC 1846.

The distance modulus and colour excess obtained for the fit described above are $\mu = 18.37$ and $E(V-I) = 0.045$. These are both slightly lower than the canonical values for the LMC; a similar effect was noted by Mucciarelli et al. (2007) when fitting Padova isochrones to their CMD for NGC 1978.

Fig. 8 shows the best-fitting BaSTI isochrones. For these models we did not have the luxury of fine sampling in metal abundance; however, $Z = 0.008$ is close to the best-fitting Padova metallicity, and provides adequate results. The best-fitting BaSTI isochrones are somewhat older than those for the Padova models – we found $\tau_u = 2.2$ Gyr for the upper turn-off and $\tau_l = 2.5$ Gyr for the lower turn-off. Uncertainties are similar to those for the Padova model fitting. The RGB, RC, and width of the SGB are slightly more successfully matched than with the best-fitting Padova isochrones; however, the turn-off regions are not quite as well matched. This may be an artifact of having a slightly incorrect metallicity for the BaSTI models. The distance modulus and colour excess obtained for the fit are $\mu = 18.57$ and $E(V-I) = 0.075$. In this case, the distance modulus is slightly higher than the canonical LMC value.

While our two pairs of measured absolute ages show an offset of ~ 0.7 Gyr, both sets of models show that the appearance of the NGC 1846 CMD can successfully be reproduced by adopting two stellar populations of the same metallicity and a difference in age of ≈ 300 Myr. Our derived metallicity [M/H] ≈ -0.40 is consistent with the spectroscopic iron abundance measured recently by Grocholski et al. (2006) from a sample of 17 RGB stars.

4 DISCUSSION AND CONCLUSIONS

Our HST/ACS photometry of the rich intermediate-age LMC cluster NGC 1846 has revealed an unusual CMD, exhibiting two main sequence turn-offs, but otherwise narrow and clearly defined primary features (RGB, SGB, RC). By examining the spatial distributions of the two sets of turn-off stars, we have shown that both are unequivocally associated with the cluster rather than any field-star population. The set of upper turn-off stars is possibly more centrally concentrated than that of the set of lower turn-off stars, and may be asymmetrically distributed. Even so, the two sets of turn-off stars share an approximately common centre. Via careful fitting of isochrones from two different groups of stellar evolution models (Padova and BaSTI), we have demonstrated that the observed features on the CMD can be explained by assuming that NGC 1846 harbours two stellar populations of the same metal abundance ([M/H] ≈ -0.40) but differing in age by ≈ 300 Myr. The absolute ages of the two populations are $\tau_u = 1.9 \pm 0.1$ Gyr and $\tau_l = 2.2 \pm 0.1$ Gyr. These are a straight average of the ages from the two different isochrone sets, and the uncertainties represent the approximate random uncertainties associated with the fitting process. We note that additional, larger systematic uncertainties are likely present – the two pairs of absolute ages are offset by 0.7 Gyr between the two sets of isochrones.

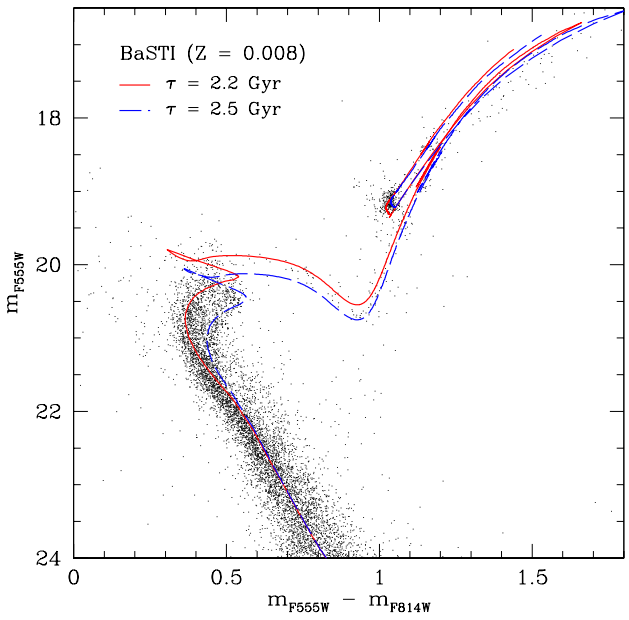

Figure 8. Best-fitting BaSTI isochrones overplotted on the cluster CMD. The upper and lower turn-off isochrones have the same metal abundance $Z = 0.008$, and ages $\tau_u = 2.2$ Gyr and $\tau_l = 2.5$ Gyr, respectively. Both have been shifted by $E(V - I) = 0.075$ and $\mu = 18.57$ to achieve the best-fitting alignment.

Given these results, it is natural to ask how such an object as NGC 1846 might have been formed. We can think of two options – either this cluster underwent two distinct episodes of star formation separated by 300 Myr, or it is the result of the merger of two star clusters formed 300 Myr apart.

Regarding the possibility that NGC 1846 underwent two separate episodes of star formation, it is difficult to see how it can have retained enough gas for this to happen. There is strong evidence that the combined effects of massive stellar winds and supernova explosions expel any remaining gas from a very young star cluster within only a few Myr (e.g., Bastian & Goodwin 2006), leading to strong changes in the cluster's internal dynamics and structure (see e.g., Goodwin & Bastian 2006, and references therein). A cluster must be very massive to retain any gas in its potential well. The only clusters where multiple episodes of star formation appear evident are globular clusters at the very upper end of the globular cluster mass function, such as ω Centauri (e.g., Villanova et al. 2007), and G1 in M31 (Meylan et al. 2001). NGC 1846 does not fulfil this criterion. Furthermore, in all such cases where multiple episodes of star formation have taken place, self-enrichment has apparently occurred. The timescale for such enrichment is not well defined; however, it seems possible that 300 Myr could be long enough given that significant chemical processing must have already occurred in the most massive cluster stars (in particular in type II supernovae and massive asymptotic giant branch stars), within the first ~ 100 Myr. It is therefore not clear why the two populations in NGC 1846 should apparently have the same metal abundance.

The merger scenario fares better. It is well known that both the LMC and SMC possess populations of candidate binary (and multiple) star clusters (e.g., Bhatia & Hatzidimitriou 1988; Hatzidimitriou & Bhatia 1990), and by using statistical arguments it can be shown that a significant fraction of these are likely to be physically linked (Bhatia & Hatzidimitriou 1988). Gravitationally bound star clusters are predicted to merge on timescales of tens of Myr to a few hundred Myr (e.g., Portegies Zwart & Rusli 2006), which is roughly consistent with the observed age difference between the two populations in NGC 1846. Old binary pairs – such as SL 349-SL 353 with an age $\sim$ 500 Myr – are certainly observed in the LMC (Leon, Bergond & Vallenari 1999). However, theories for the formation of bound binary star clusters (e.g., Fujimoto & Kumai 1997) suggest that such objects should be roughly coeval, with age differences less than ≈ 100 Myr at most. This is inconsistent with the observed populations in NGC 1846, and indeed with several known binary pairs in the LMC – such as SL 356-SL 357, which have ages of 70 Myr and 600 Myr, respectively (Leon et al. 1999).

One way to circumvent this is if some clusters are formed in star cluster groups (SCGs) in giant molecular clouds (see e.g., Leon et al. 1999, and references therein). In such complexes, cluster formation can be spread over several hundred Myr. Furthermore, clusters observed to be physically associated at present do not have to have been formed this way, as the cross-section for tidal capture is much increased due to the relatively high density of star clusters within the SCG. This scenario therefore allows for the existence of cluster pairs which are older than the typical timescale for merging, as well as for cluster pairs with large age differences, both of which types are seen in the LMC. If the two components of NGC 1846 were formed in a SCG in the same giant molecular cloud, this also naturally explains their matching metal abundances.

In this scenario, the two clusters comprising the present day NGC 1846 must have merged less than $1.5 - 2.2$ Gyr ago, based on our derived ages for the upper turn-off population. The median relaxation time in intermediate-age LMC clusters is typically of order $1 - 2$ Gyr (e.g., Mackey et al. 2007); the central relaxation time may be up to a factor ten shorter than this. The very inner region of NGC 1846 is therefore quite possibly dynamically old enough for two merging clusters to now be sharing a common centre and be fairly well mixed through relaxation processes; however it is probable that asymmetries could still exist outside the core, as our observations have hinted. It would be extremely interesting to investigate the evolution of a merged LMC-type cluster via realistic N-body modelling to examine if the observed features of NGC 1846 can be reproduced. Such calculations may allow the time when merging occurred to be constrained – this would be extremely useful in the context of examining the SCG scenario. Direct N-body modelling of LMC-type clusters is now possible – Mackey et al. (2007) present models with $N = 10^5$ particles integrated over a Hubble time of evolution. Since we do observe asymmetries in the distribution of the two populations in NGC 1846, dynamical signatures offering clues to the formation process may also still be present outside the cluster centre. It would certainly be interesting (although observationally challenging) to investigate the internal dynamics of this object. N-body modelling would be helpful in this regard as

it would allow the expected level of the signature to be predicted. NGC 1846 patently warrants further study, including improved photometry of the turn-off region, for important insights into star cluster formation processes.

ACKNOWLEDGEMENTS

We are grateful to Annette Ferguson for reading through a draft of this paper and offering helpful comments and suggestions. ADM is supported by a Marie Curie Excellence Grant from the European Commission under contract MCEXT-CT-2005-025869. This paper is based on observations made with the NASA/ESA Hubble Space Telescope, obtained at the Space Telescope Science Institute, which is operated by the Association of Universities for Research in Astronomy, Inc., under NASA contract NAS 5-26555. These observations are associated with program #9891.

REFERENCES

Bastian N., Goodwin S. P., 2006, MNRAS, 369, L9
Bedin L.R., Cassisi S., Castelli F., Piotto G., Anderson J., Salaris M., Momany Y., Pietrinferni A., 2005, MNRAS, 357, 1048
Bhatia R., Hatzidimitriou D., 1988, MNRAS, 230, 215
Dolphin, A. E. 2000, PASP, 112, 1383
Fujimoto M., Kumai Y., 1997, AJ, 113, 249
Girardi L., Bressan A., Bertelli G., Chiosi C., 2000, A&AS, 141, 371
Goodwin S. P., Bastian N., 2006, MNRAS, 373, 752
Grocholski A. J., Cole A. A., Sarajedini A., Geisler D., Smith V. V., 2006, AJ, 132, 1630
Hatzidimitriou D., Bhatia R. K., 1990, A&A, 230, 11
Leon S., Bergond G., Vallenari A., 1999, A&A, 344, 450
Mackey A. D., Gilmore G. F., 2003, MNRAS, 338, 85
Mackey A. D., Gilmore G. F., 2004, MNRAS, 352, 153
Mackey A. D., Payne M. J., Gilmore G. F., 2006, MNRAS, 369, 921
Mackey A. D., Wilkinson M. I., Davies M. B., Gilmore G. F., 2007, MNRAS, submitted
Meylan G., Sarajedini A., Jablonka P., Djorgovski S., Bridges T., Rich R., 2001, AJ, 122, 830
Mucciarelli A., Ferraro F. R., Origlia L., Fusi Pecci F., 2007, AJ, in press
Olszewski E. W., Schommer R. A., Suntzeff N. B., Harris H. C., 1991, AJ, 101, 515
Pietrinferni A., Cassisi S., Salaris M., Castelli F., 2004, ApJ, 612, 168
Portegies Zwart S. F., Rusli S. P., 2006, MNRAS, 374, 931
Sirianni M., et al. 2005, PASP, 117, 1049
Villanova S., et al., 2007, ApJ, in press

This paper has been typeset from a TEX/ LATEX file prepared by the author.